

Measurement-induced phase transition for free fermions above one dimension

Igor Poboiko,^{1,2} Igor V. Gornyi,^{1,2} and Alexander D. Mirlin^{1,2}

¹*Institute for Quantum Materials and Technologies, Karlsruhe Institute of Technology, 76021 Karlsruhe, Germany*

²*Institut für Theorie der Kondensierten Materie, Karlsruhe Institute of Technology, 76128 Karlsruhe, Germany*

(Dated: September 25, 2023)

A theory of the measurement-induced entanglement phase transition for free-fermion models in $d > 1$ dimensions is developed. The critical point separates a gapless phase with $\ell^{d-1} \ln \ell$ scaling of the second cumulant of the particle number and of the entanglement entropy and an area-law phase with ℓ^{d-1} scaling, where ℓ is a size of the subsystem. The problem is mapped onto an $SU(R)$ replica non-linear sigma model in $d + 1$ dimensions, with $R \rightarrow 1$. Using renormalization-group analysis, we calculate critical indices in one-loop approximation justified for $d = 1 + \epsilon$ with $\epsilon \ll 1$. Further, we carry out a numerical study of the transition for a $d = 2$ model on a square lattice, determine numerically the critical point, and estimate the critical index of the correlation length, $\nu \approx 1.8 - 2.2$.

Introduction—Quantum dynamics of many-body systems subjected to quantum measurements and, in particular, measurement-induced entanglement phase transitions attract a great deal of research attention. This area of research connects the condensed matter physics with quantum information processing. Measurement-induced transitions, which result from a competition between unitary dynamics that enhances the entanglement and measurements that reduce it, were initially investigated in quantum-circuit framework [1–25]. Later works showed ubiquity of measurement-induced transitions; they were studied in a variety of many-body systems, including free fermions [26–42], Majorana fermions [43–45], Ising spin systems [46–55], Bose-Hubbard models [56–60], disordered systems with Anderson or many-body localization [35, 61, 62], and models of Sachdev-Ye-Kitaev type [63, 64]. While most of the studies were of computational character, important analytical progress has been achieved for some of the models. Furthermore, recent works on trapped-ion systems [65] and superconducting quantum processors [66] reported experimental realizations of measurement-induced phase transitions.

Recently, the present authors developed a field-theoretical approach to the measurement-induced physics in the model of one-dimensional free fermions [42]. The problem was mapped onto a two-dimensional $SU(R)$ non-linear sigma-model (NLSM) in the replica limit $R \rightarrow 1$. This allowed us to show that this system is always in the area-law phase but, for small measurement rate, exhibits a broad intermediate regime with logarithmic increase of the entropy. These analytical results were supported by numerical simulations.

In the present work, we show that, in spatial dimensionality $d > 1$, the system of free fermions subjected to measurements exhibits a phase transition between a gapless phase with $\ell^{d-1} \ln \ell$ scaling of the second cumulant of the particle number and of the entanglement entropy and an area-law phase with ℓ^{d-1} scaling. (Here ℓ is a size of the subsystem.) On the analytical side, we map the problem onto a replica NLSM in $d + 1$ dimensions and, in this framework, develop a renormalization group (RG)

analysis of the transition. We calculate critical indices in one-loop approximation, which is parametrically justified for $d = 1 + \epsilon$ with $\epsilon \ll 1$. On the computational side, we study the transition in $d = 2$ dimensions, determine numerically the critical point, and estimate the correlation-length critical exponent ν .

Model and measurement protocol—We consider a d -dimensional tight-binding model of free fermions, defined on a hypercubic lattice with L^d sites and periodic boundary conditions. The system Hamiltonian reads:

$$\hat{H} = -J \sum_{\langle \mathbf{x}, \mathbf{x}' \rangle} [\hat{\psi}^\dagger(\mathbf{x}) \hat{\psi}(\mathbf{x}') + h.c.], \quad (1)$$

where summation is performed over lattice links and the hopping constant J defines the energy scale. Each site \mathbf{x} of the system is projectively monitored: at randomly chosen times $t_i^{(\mathbf{x})}$ sampled from a Poissonian distribution with a rate γ , independently for each site, a projective measurement of the site occupation number $\hat{n}(\mathbf{x}) = \hat{\psi}^\dagger(\mathbf{x}) \hat{\psi}(\mathbf{x})$ is performed. The outcome of such measurements, which can be either zero or unity, $n = 0, 1$, is random, with probabilities determined by the many-body wave function Ψ at time $t = 0$:

$$\text{Prob}(n | \langle \mathbf{x}, t \rangle) = \langle \Psi(t=0) | \hat{\mathbb{P}}_n(\mathbf{x}) | \Psi(t=0) \rangle. \quad (2)$$

This standard quantum-mechanical Born rule involves many-body projectors onto linear subspaces with a definite site occupation $n = 0, 1$:

$$\hat{\mathbb{P}}_0(\mathbf{x}) = 1 - \hat{n}(\mathbf{x}), \quad \hat{\mathbb{P}}_1(\mathbf{x}) = \hat{n}(\mathbf{x}). \quad (3)$$

After the measurement at time t on site \mathbf{x} with an outcome n is performed, the wavefunction undergoes a Neumann collapse and is projected onto the corresponding subspace with subsequent renormalization:

$$|\Psi(t+0)\rangle = \frac{\hat{\mathbb{P}}_n(\mathbf{x}) |\Psi(t=0)\rangle}{\|\hat{\mathbb{P}}_n(\mathbf{x}) |\Psi(t=0)\rangle\|}. \quad (4)$$

The system is initially prepared in an arbitrary Gaussian pure state (i.e., described by a Slater determinant)

$|\Psi(t_0)\rangle$. The evolution consists of unitary part governed by the Hamiltonian \hat{H} and non-unitary part introduced by measurements according to the above protocol. We will study properties of the wavefunction $|\Psi(t=0)\rangle$ in the limit $t_0 \rightarrow -\infty$ (“steady state”). This pure state depends, by construction, on the random “measurement trajectory” $\mathcal{T} = \{t_m, \mathbf{x}_m, n_m\}$.

To investigate the measurement-induced entanglement transition, we utilize a relation [67] between the entanglement entropy \mathcal{S}_E for a given subsystem A (characterized by the reduced density matrix $\hat{\rho}_A$) and an infinite series of particle-number cumulants,

$$\mathcal{C}_A^{(N)} = \left\langle \left\langle \left(\sum_{\mathbf{x} \in A} \hat{n}(\mathbf{x}) \right)^N \right\rangle \right\rangle, \quad (5)$$

in the same subsystem. This relation,

$$\mathcal{S}_E \equiv -\text{Tr}(\hat{\rho}_A \ln \hat{\rho}_A) = \sum_{q=1}^{\infty} 2\zeta(2q) \mathcal{C}_A^{(2q)} \quad (6)$$

with ζ the zeta-function, holds for arbitrary pure Gaussian states, including [35, 40, 42] monitored systems. Moreover, it was demonstrated [42] that the first term (involving the second particle-number cumulant $\mathcal{C}_A^{(2)}$) is dominant in the series (6), i.e., $\mathcal{S}_E \approx (\pi^2/3) \mathcal{C}_A^{(2)}$. This approximation is parametrically controlled for small measurement rate γ/J and holds numerically with an excellent precision even when γ/J is not small. This property is also known to hold in disordered systems [68], even in the vicinity of the Anderson metal-insulator transition. Notably, the present problem bears a certain similarity to that of Anderson transitions [69], as both can be mapped to corresponding NLSMs, albeit with different replica limits. For these reasons, our further analysis focuses on the second particle-number cumulant $\mathcal{C}_A^{(2)}$, with the results applying also to the entanglement entropy \mathcal{S}_E .

Non-linear sigma model—In Ref. [42], it was shown that the behavior of the particle-number cumulants (and of the entanglement entropy) in monitored one-dimensional free-fermion systems is described by a replicated NLSM (see also Refs. [24, 43] for related NLSMs in different setups involving Majorana fermions). Specifically, this field theory operates with matrix fields $\hat{U}(\mathbf{x}, t) \in \text{SU}(R)$ in the replica space, governed by the Lagrangian density

$$\mathcal{L}[\hat{U}, \hat{\Xi}] = \frac{g}{2} \text{Tr} \left(\frac{1}{v_0} \partial_t^{\Xi} \hat{U} (\partial_t^{\Xi} \hat{U})^\dagger + v_0 \nabla \hat{U} \nabla \hat{U}^\dagger \right), \quad (7)$$

and yields the observable correlation functions in the replica limit $R \rightarrow 1$ (dictated by the Born rule). The derivation of the effective theory (7) is straightforwardly extended to arbitrary spatial dimensionality d ; as a result, we obtain the NLSM in $d+1$ dimensions [70]. The theory is defined in the time domain $t \leq 0$, with the boundary condition $\hat{U}(\mathbf{x}, t=0) = \hat{\mathbb{1}}$. As a consequence

of the measurement-induced infinite-temperature heating of the system in the steady state, v_0 in Eq. (7) is a root-mean-square group velocity averaged over the Brillouin zone, $v_0 = \sqrt{2}J$. The bare value of the coupling constant g is given by:

$$g_0 = \rho(1-\rho)v_0/\gamma \quad (8)$$

with $\rho \in [0, 1]$ being an average filling factor of the state (which is conserved during the evolution). The time derivative in Eq. (7) contains a source matrix field $\hat{\Xi}(\mathbf{x}, t)$, which is diagonal with respect to replica indices, $\hat{\Xi} = \text{diag}(\{\Xi_r\}_{r=1}^R)$:

$$\partial_t^{\Xi} \hat{U} \equiv \partial_t \hat{U} + (iZ/2)\{\hat{U}, \hat{\Xi}\}. \quad (9)$$

Here $\{\cdot, \cdot\}$ is the anticommutator and we have also introduced a renormalization factor Z with the bare value $Z_0 = 1$.

The generating functional $\mathcal{Z}[\hat{\Xi}]$ obtained from Eq. 7 in the presence of the source is then used to calculate the density correlation function that determines the particle-number cumulants in Eq. (6). The simplest, two-point correlation function is given by

$$\begin{aligned} C(\mathbf{x}) &= \overline{\{\hat{n}(\mathbf{x}), \hat{n}(0)\}/2} - \overline{\hat{n}(\mathbf{x})} \overline{\hat{n}(0)} \\ &= -\lim_{\substack{t, t' \rightarrow 0 \\ R \rightarrow 1}} \frac{1}{R-1} \left[\frac{g_0}{v_0} \delta(\mathbf{x}) \delta(t-t') + \sum_{r=1}^R \frac{\delta^2 \ln \mathcal{Z}[\hat{\Xi}]}{\delta \Xi_r(\mathbf{x}, t) \delta \Xi_r(0, t')} \right], \end{aligned} \quad (10)$$

where the overbar denotes averaging over quantum trajectories \mathcal{T} . On the Gaussian level, this correlation function and its Fourier transform read:

$$C(\mathbf{x}) = -2g_0/\sigma_d |\mathbf{x}|^{d+1}, \quad C(\mathbf{q}) = g_0 |\mathbf{q}|, \quad (11)$$

where $\sigma_d = 2\pi^{(d+1)/2}/\Gamma(d/2+1/2)$ is the surface area of d -dimensional sphere (with Γ the gamma function). For a subsystem in the form of a (d -dimensional) ball of radius ℓ , this correlation function leads to the following behavior of the second cumulant in the Gaussian approximation:

$$\mathcal{C}_\ell^{(2)} \simeq \frac{g_0}{\pi} \sigma_{d-1} \ell^{d-1} \ln \frac{\ell}{l_0}, \quad (12)$$

where $l_0 \simeq J/\gamma\sqrt{2}$ is the mean free path that plays a role of the ultraviolet cutoff for the NLSM. Importantly, a power-law (“critical”) character (11) of $C(\mathbf{x})$ leads to a logarithmic enhancement of $\mathcal{C}_\ell^{(2)}$ and of the entanglement entropy in comparison to area law.

RG and scaling analysis—The long-wavelength behavior of the NLSM (7) can be analyzed by means of RG equations for two running dimensionless coupling constants, $G(\ell) = g(\ell)\ell^{d-1}$ and $Z(\ell)$. Since $d+1=2$ is a logarithmic dimension for the NLSM theory, we can develop an ϵ -expansion with $\epsilon = d-1$. In the one-loop

approximation, the RG flow is described by (cf. Ref. [42] where $\epsilon = 0$):

$$dG/d\ln\ell \equiv \beta(G) = \epsilon G - R/4\pi + O(1/G), \quad (13)$$

$$d\ln Z/d\ln\ell \equiv \beta_Z(G) = O(1/G^2). \quad (14)$$

For spatial dimensions higher than unity, $\epsilon > 0$, Eq. (13) implies the existence of a critical point defined by the condition $\beta(G_c) = 0$. Following an analogy with the Anderson metal-insulator transition, we will call the phase governed by an infrared-stable fixed point $G = 0$ “insulating”, which corresponds to the area-law phase in the context of measurement-induced phase transitions. The phase with $G \rightarrow \infty$ will be referred to as “metallic,” where the scaling of the cumulant with ℓ will be given by Eq. (12) with a renormalized prefactor. In the replica limit $R \rightarrow 1$ and to leading order in $\epsilon \ll 1$, we find the critical point separating these two phases at

$$G_c \approx 1/4\pi\epsilon + O(\epsilon^0), \quad (15)$$

akin to the critical conductance in Anderson transitions [69, 71–73].

Expanding RG equations (13) and (14) around the critical point, $\beta(G) \approx \beta'(G_c)(G - G_c) \equiv (G - G_c)/\nu$ and $\beta_Z(G) \approx \beta_Z(G_c) \equiv \zeta/2$, we obtain the following one-loop results for the corresponding critical exponents:

$$\nu = 1/\epsilon + O(\epsilon^0), \quad \zeta = 0 + O(\epsilon^2). \quad (16)$$

We will argue below that ζ is in fact exactly zero but we keep it here for generality. Integration of the RG equations in the vicinity of the critical point yields:

$$G(\ell) - G_c \approx (G_0 - G_c) \cdot (\ell/l_0)^{1/\nu}, \quad Z(\ell) \approx (\ell/l_0)^{\zeta/2}. \quad (17)$$

The length scale at which $|G - G_c| \sim G_c$ defines the correlation length:

$$l_{\text{corr}} \sim l_0 (|G_0 - G_c|/G_c)^{-\nu}. \quad (18)$$

The two-point density correlation function (10) is given (in the Fourier space) by its mean-field expression (11) with the renormalized values of g and Z taken at the length scale $\ell \sim q^{-1}$:

$$C(q) = Z^2(q^{-1})g(q^{-1})q = Z^2(q^{-1})G(q^{-1})q^d. \quad (19)$$

This gives the scaling ansatz valid in the critical region in the vicinity of the transition at $G_0 = G(l_0) \approx G_c$:

$$C(q) = G_c q^d (ql_0)^{-\zeta} f(ql_{\text{corr}}), \quad (20)$$

with a scaling functions $f(k)$ with two branches describing both sides of the transition. The $k \gg 1$ behavior of $f(k)$ describes the critical point and its vicinity. According to Eq. (17), we have

$$f(k \gg 1) \approx \begin{cases} 1 + k^{-1/\nu}, & G_0 > G_c, \\ 1 - k^{-1/\nu}, & G_0 < G_c. \end{cases} \quad (21)$$

The $k \ll 1$ behavior of $f(k)$ corresponds to the “metallic” and “insulating” phases. On the “metallic” side of the transition, Eq. (20) should reproduce the asymptotics $C(q) \propto q$. In the area-law phase, one expects $C(\mathbf{x})$ to decay sufficiently fast (e.g., exponentially) at infinity, so that its Fourier transform should be analytic, implying $C(q) \propto q^2$. To match this asymptotic behavior, the scaling function should satisfy

$$f(k \ll 1) \sim \begin{cases} 1/k^{d-1-\zeta}, & G_0 > G_c, \\ k^{2-d+\zeta}, & G_0 < G_c. \end{cases} \quad (22)$$

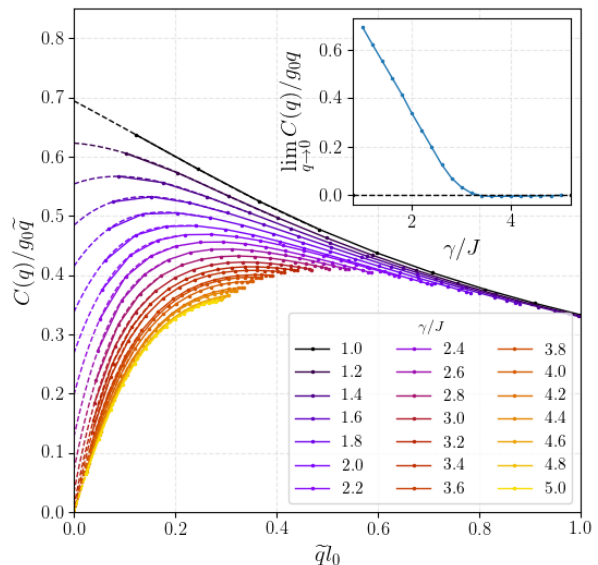


FIG. 1. Correlation function $C(q)$ of an $L \times L$ system with $L = 36$ across the transition. Shown are dependencies of $C(q)/g_0\tilde{q}$ on \tilde{q}_0 [with $\tilde{q} = 2 \sin(q/2)$] for values of the measurement rate γ/J from 1.0 to 5.0. Dashed lines: cubic polynomial extrapolation down to $q \rightarrow 0$ using 5 lowest momenta. Inset: the extrapolated value at $q \rightarrow 0$ as a function of γ/J . For $\gamma > \gamma_c$, where $\gamma_c/J \simeq 3.5$, the extrapolated value is zero within numerical precision, which is a manifestation of the measurement-induced phase transition.

Numerical analysis—To verify and complement our analytical theory, we carried out direct numerical simulations of dynamics of a monitored two-dimensional free-fermion system following the protocol outlined above. As the protocol preserves the Gaussian nature of the state, the system is fully characterized by the single-particle Green function $\mathcal{G}_{\mathbf{x}\mathbf{x}'} \equiv \langle \hat{\psi}^\dagger(\mathbf{x}) \hat{\psi}(\mathbf{x}') \rangle$. Executing unitary evolution along with projective measurements until the system has reached the steady state, we evaluated the two-point density correlation function on a lattice:

$$C_{\mathbf{x}\mathbf{x}'} = \langle \hat{n}(\mathbf{x}) \hat{n}(\mathbf{x}') \rangle - \langle \hat{n}(\mathbf{x}) \rangle \langle \hat{n}(\mathbf{x}') \rangle = \mathcal{G}_{\mathbf{x}\mathbf{x}} \delta_{\mathbf{x}\mathbf{x}'} - \mathcal{G}_{\mathbf{x}\mathbf{x}'} \mathcal{G}_{\mathbf{x}'\mathbf{x}}. \quad (23)$$

The protocol was repeated ~ 100 times, and averaging over quantum trajectories and over positions in the sample was performed to calculate $C(\mathbf{x} - \mathbf{x}') = \overline{C_{\mathbf{x}\mathbf{x}'}}$.

The results obtained for an $L \times L$ system with periodic boundary conditions and $L = 36$ are shown in Fig. 1. According to the above analytical discussion, the transition can be characterized by the behavior of $\lim_{q \rightarrow 0} C(q)/q$, which is expected to be finite in the “metallic” phase and zero in the “insulating” phase (where $C(q) \propto q^2$). The $q \rightarrow 0$ values extrapolated from the finite-size curves (see inset) are fully consistent with this prediction, yielding an estimate $\gamma_c/J \approx 3.5$ for the critical point. Furthermore, at $\gamma \rightarrow 0$, the Gaussian approximation (11) is parametrically justified and predicts that $C(q)/g_0q$ should saturate at unity, which is also in excellent agreement with the numerical data.

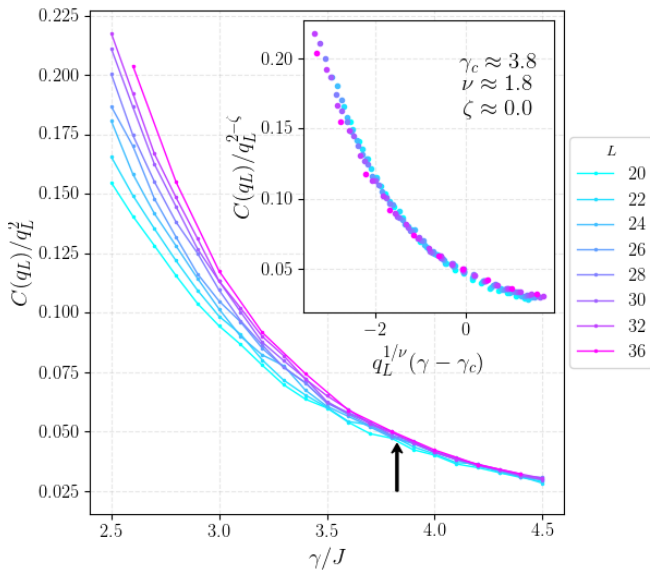


FIG. 2. The ratio $C(q_L)/q_L^2$ as a function of γ/J for system sizes L from 20 to 36. Arrow marks the estimated position of the transition. Inset: collapse according to Eq. (20) with a scaling function $f(k = x^{-\nu})$, where x is the x -axis of the inset. Obtained values of γ_c , ν , and ζ are shown.

To explore the transition more accurately, we focus now on a narrower vicinity of the critical point. According to Eqs. (20), (18), the data for $C(q)/q^d$ should collapse, with the suitable choice of γ_c and critical exponents ν and ζ , on a single universal function $f(k)$. Figure 2 demonstrates the behavior of the ratio $C(q)/q^2$ at the smallest momentum available for a finite system, $q_L \equiv 2\pi/L$ for system sizes from $L = 20$ to $L = 36$ as a function of γ . As shown in the inset, a good collapse can indeed be achieved, yielding a more accurate estimate for the transition point, $\gamma_c/J \approx 3.8$, and the critical

exponents $\zeta \approx 0.0$ and $\nu \approx 1.8$.

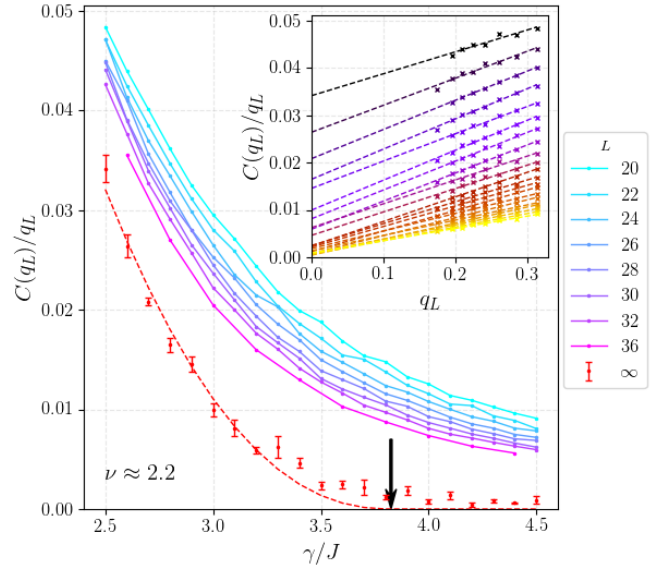


FIG. 3. Ratio $C(q)/q$ for the smallest available momentum $q = q_L \equiv 2\pi/L$ for system sizes L from 20 to 36, as a function of γ/J close to the transition. Red dots with error bars: extrapolation to $L \rightarrow \infty$. Red dashed curve: critical behavior with $\nu = 2.2$. Arrow marks the estimated γ_c . Inset: extrapolation to $q_L \rightarrow 0$ for γ/J ranging between 2.5 (top) and 4.5 (bottom) with step 0.1.

As an alternative way to analyze the data, we show in Fig. 3 the ratio $C(q_L)/q_L$ for various L , with an extrapolation to $L \rightarrow \infty$ (i.e., $q_L \rightarrow 0$). We observe that for $\gamma/J \geq 3.8$ the extrapolated value stops varying (up to statistical fluctuations ~ 0.01) and becomes equal to zero with this accuracy, confirming the above identification of the transition point, $\gamma_c/J \approx 3.8$. Further, according to Eq. (20), the density correlation function scales as $C(q) \sim q^{2-\zeta}$ at $\gamma = \gamma_c$. Our data yield $\zeta \approx 0$ within numerical accuracy, in agreement with the scaling collapse.

To find ν , we use Eq. (19) that predicts the following behavior on the “metallic” side of the transition ($\gamma < \gamma_c$) in the thermodynamic limit:

$$\lim_{L \rightarrow \infty} C(q_L)/q_L \simeq (G_0 - G_c)^{\nu(d-1-\zeta)} \propto (\gamma_c - \gamma)^{\nu(1-\zeta)}, \quad (24)$$

where we set $d = 2$ in the last expression. Fitting the numerical results in Fig. 3 and setting $\zeta = 0$, we obtain an estimate $\nu \approx 2.2$, in good agreement with the value found from the scaling collapse.

Exactness of $\zeta = 0$. Mutual information — We have found that $\zeta = 0$ to one-loop order and $\zeta \approx 0$ numerically. We show now that $\zeta = 0$ is exact. According to Eq. (10), $C(\mathbf{x} - \mathbf{x}')$ at $\mathbf{x} \neq \mathbf{x}'$ is a correlation function of Noether currents $\hat{\mathcal{J}}_t = (-i/2)(\hat{U}^\dagger \partial_t \hat{U} - \hat{U} \partial_t \hat{U}^\dagger)$ at

\mathbf{x} and \mathbf{x}' . Thus, within the Anderson-transition analogy, $-C(\mathbf{x} - \mathbf{x}')$ has a meaning of two-point conductance. Consider two spatial regions A and B , both of extension $\sim \ell$ in each direction and separated by a distance ℓ , and define a “two-terminal conductance” $G_{AB} = -\int_A d^d \mathbf{x} \int_B d^d \mathbf{x}' C(\mathbf{x} - \mathbf{x}')$. At criticality, G_{AB} must be an ℓ -independent constant $\sim G_c$. This implies that $C(\mathbf{x} - \mathbf{x}') \propto |\mathbf{x} - \mathbf{x}'|^{-2d}$ and thus $\zeta = 0$, cf. an analogous argument (with $d = 1$) for quantum Hall transitions in Ref. [74]. On a more general level, it is known that surface integrals of conserved currents are symmetry generators [75] and thus have scaling dimension zero at criticality [76, 77]. Thus, our currents \hat{J}_t should have scaling dimension d , implying again that $C(\mathbf{x} - \mathbf{x}') \propto |\mathbf{x} - \mathbf{x}'|^{-2d}$.

Note that $-G_{AB}$ in our problem is a covariance of the particle numbers in systems A and B . Extending a discussion below Eq. (6), we relate it to the quantum mutual information between A and B [70]. According to our findings, G_{AB} scales as ℓ^{d-1} , constant, and $e^{-\ell/\ell_{\text{corr}}}$ for $\gamma < \gamma_c$, $\gamma = \gamma_c$, and $\gamma > \gamma_c$, respectively.

Summary—We have developed a field theory for monitored d -dimensional free-fermion systems, which has a form of an $SU(R)$ NLSM in $d + 1$ dimensions, with the $R \rightarrow 1$ replica limit. By performing its RG analysis, we have demonstrated the existence of a measurement-induced entanglement phase transition in such models for dimensions $d > 1$. The transition point separates a symmetry-broken “metallic” phase realized for rare measurements and characterized by $\ell^{d-1} \ln \ell$ scaling of the second particle-number cumulant and the entanglement entropy from the “insulating” area-law phase for frequent measurements. We have further calculated critical indices in the one-loop order of ϵ -expansion in $d = 1 + \epsilon$ dimensions. Additionally, numerical investigation of the $d = 2$ model on a square lattice enabled us to pinpoint the critical point and to estimate the correlation-length exponent $\nu \approx 1.8 - 2.2$. The measurement-induced entanglement transition for free fermions in dimensions $d > 1$ bears a striking similarity to Anderson metal-insulator transition in disordered systems of $d + 1$ dimensions. In the present context, it is the quantum information (closely related to particle-number fluctuations) that experiences localization. As future important generalizations of the theory, we envisage inclusion of interaction and/or of static disorder, as well as measurement protocols generating non-trivial topology.

Acknowledgments—We are grateful to A. Altland, D. Bernard, M. Buchhold, K. Chahine, S. Diehl, E. Doggen, Y. Gefen, I. Gruzberg, P. Ostrovsky, P. Pöpperl, and M. Szyniszewski for fruitful discussions. We acknowledge support by the Deutsche Forschungsgemeinschaft (DFG) via the grants MI 658/14-1 and GO 1405/6-1.

Note added—We have learned about a parallel related activity by K. Chahine and M. Buchhold.

-
- [1] Y. Li, X. Chen, and M. P. A. Fisher, Quantum Zeno effect and the many-body entanglement transition, *Phys. Rev. B* **98**, 205136 (2018).
 - [2] B. Skinner, J. Ruhman, and A. Nahum, Measurement-induced phase transitions in the dynamics of entanglement, *Phys. Rev. X* **9**, 031009 (2019).
 - [3] A. Chan, R. M. Nandkishore, M. Pretko, and G. Smith, Unitary-projective entanglement dynamics, *Phys. Rev. B* **99**, 224307 (2019).
 - [4] M. Szyniszewski, A. Romito, and H. Schomerus, Entanglement transition from variable-strength weak measurements, *Phys. Rev. B* **100**, 064204 (2019).
 - [5] Y. Li, X. Chen, and M. P. A. Fisher, Measurement-driven entanglement transition in hybrid quantum circuits, *Phys. Rev. B* **100**, 134306 (2019).
 - [6] Y. Bao, S. Choi, and E. Altman, Theory of the phase transition in random unitary circuits with measurements, *Phys. Rev. B* **101**, 104301 (2020).
 - [7] S. Choi, Y. Bao, X.-L. Qi, and E. Altman, Quantum error correction in scrambling dynamics and measurement-induced phase transition, *Phys. Rev. Lett.* **125**, 030505 (2020).
 - [8] M. J. Gullans and D. A. Huse, Dynamical purification phase transition induced by quantum measurements, *Phys. Rev. X* **10**, 041020 (2020).
 - [9] M. J. Gullans and D. A. Huse, Scalable probes of measurement-induced criticality, *Phys. Rev. Lett.* **125**, 070606 (2020).
 - [10] C.-M. Jian, Y.-Z. You, R. Vasseur, and A. W. W. Ludwig, Measurement-induced criticality in random quantum circuits, *Phys. Rev. B* **101**, 104302 (2020).
 - [11] A. Zabalo, M. J. Gullans, J. H. Wilson, S. Gopalakrishnan, D. A. Huse, and J. H. Pixley, Critical properties of the measurement-induced transition in random quantum circuits, *Phys. Rev. B* **101**, 060301(R) (2020).
 - [12] J. Iaconis, A. Lucas, and X. Chen, Measurement-induced phase transitions in quantum automaton circuits, *Phys. Rev. B* **102**, 224311 (2020).
 - [13] X. Turkeshi, R. Fazio, and M. Dalmonte, Measurement-induced criticality in $(2+1)$ -dimensional hybrid quantum circuits, *Phys. Rev. B* **102**, 014315 (2020).
 - [14] L. Zhang, J. A. Reyes, S. Kourtis, C. Chamon, E. R. Mucciolo, and A. E. Ruckenstein, Nonuniversal entanglement level statistics in projection-driven quantum circuits, *Phys. Rev. B* **101**, 235104 (2020).
 - [15] A. Nahum, S. Roy, B. Skinner, and J. Ruhman, Measurement and entanglement phase transitions in all-to-all quantum circuits, on quantum trees, and in Landau-Ginsburg theory, *PRX Quantum* **2**, 010352 (2021).
 - [16] M. Ippoliti, M. J. Gullans, S. Gopalakrishnan, D. A. Huse, and V. Khemani, Entanglement phase transitions in measurement-only dynamics, *Phys. Rev. X* **11**, 011030 (2021).
 - [17] M. Ippoliti and V. Khemani, Postselection-free entanglement dynamics via spacetime duality, *Phys. Rev. Lett.* **126**, 060501 (2021).
 - [18] A. Lavasani, Y. Alavirad, and M. Barkeshli, Measurement-induced topological entanglement transitions in symmetric random quantum circuits, *Nat. Phys.* **17**, 342 (2021).
 - [19] A. Lavasani, Y. Alavirad, and M. Barkeshli, Topologi-

- cal order and criticality in $(2 + 1)$ D monitored random quantum circuits, *Phys. Rev. Lett.* **127**, 235701 (2021).
- [20] S. Sang and T. H. Hsieh, Measurement-protected quantum phases, *Phys. Rev. Research* **3**, 023200 (2021).
- [21] M. P. Fisher, V. Khemani, A. Nahum, and S. Vijay, Random quantum circuits, *Annual Review of Condensed Matter Physics* **14**, 335 (2023).
- [22] M. Block, Y. Bao, S. Choi, E. Altman, and N. Y. Yao, Measurement-induced transition in long-range interacting quantum circuits, *Phys. Rev. Lett.* **128**, 010604 (2022).
- [23] S. Sharma, X. Turkeshi, R. Fazio, and M. Dalmonte, Measurement-induced criticality in extended and long-range unitary circuits, *SciPost Phys. Core* **5**, 023 (2022).
- [24] C.-M. Jian, H. Shapourian, B. Bauer, and A. W. W. Ludwig, Measurement-induced entanglement transitions in quantum circuits of non-interacting fermions: Born-rule versus forced measurements (2023), arXiv:2302.09094.
- [25] S. P. Kelly, U. Poschinger, F. Schmidt-Kaler, M. P. A. Fisher, and J. Marino, Coherence requirements for quantum communication from hybrid circuit dynamics (2023), arXiv:2210.11547 [quant-ph].
- [26] X. Cao, A. Tilloy, and A. De Luca, Entanglement in a fermion chain under continuous monitoring, *SciPost Phys.* **7**, 024 (2019).
- [27] O. Alberton, M. Buchhold, and S. Diehl, Entanglement transition in a monitored free-fermion chain: From extended criticality to area law, *Phys. Rev. Lett.* **126**, 170602 (2021).
- [28] X. Chen, Y. Li, M. P. A. Fisher, and A. Lucas, Emergent conformal symmetry in nonunitary random dynamics of free fermions, *Phys. Rev. Research* **2**, 033017 (2020).
- [29] Q. Tang, X. Chen, and W. Zhu, Quantum criticality in the nonunitary dynamics of $(2 + 1)$ -dimensional free fermions, *Phys. Rev. B* **103**, 174303 (2021).
- [30] M. Coppola, E. Tirrito, D. Karevski, and M. Collura, Growth of entanglement entropy under local projective measurements, *Phys. Rev. B* **105**, 094303 (2022).
- [31] B. Ladewig, S. Diehl, and M. Buchhold, Monitored open fermion dynamics: Exploring the interplay of measurement, decoherence, and free Hamiltonian evolution, *Phys. Rev. Research* **4**, 033001 (2022).
- [32] F. Carollo and V. Alba, Entangled multiplets and spreading of quantum correlations in a continuously monitored tight-binding chain, *Phys. Rev. B* **106**, L220304 (2022).
- [33] M. Buchhold, T. Müller, and S. Diehl, Revealing measurement-induced phase transitions by pre-selection (2022), arXiv:2208.10506.
- [34] Q. Yang, Y. Zuo, and D. E. Liu, Keldysh nonlinear sigma model for a free-fermion gas under continuous measurements, *Phys. Rev. Res.* **5**, 033174 (2023).
- [35] M. Szyniszewski, O. Lunt, and A. Pal, Disordered monitored free fermions (2022), arXiv:2211.02534.
- [36] M. Buchhold, Y. Minoguchi, A. Altland, and S. Diehl, Effective theory for the measurement-induced phase transition of Dirac fermions, *Phys. Rev. X* **11**, 041004 (2021).
- [37] M. Van Regemortel, Z.-P. Cian, A. Seif, H. Dehghani, and M. Hafezi, Entanglement entropy scaling transition under competing monitoring protocols, *Phys. Rev. Lett.* **126**, 123604 (2021).
- [38] Y. L. Gal, X. Turkeshi, and M. Schirò, Volume-to-area law entanglement transition in a non-Hermitian free fermionic chain (2022), arXiv:2210.11937.
- [39] H. Lóio, A. De Luca, J. De Nardis, and X. Turkeshi, Purification timescales in monitored fermions (2023), arXiv:2303.12216 [cond-mat.stat-mech].
- [40] X. Turkeshi, L. Piroli, and M. Schirò, Enhanced entanglement negativity in boundary-driven monitored fermionic chains, *Phys. Rev. B* **106**, 024304 (2022).
- [41] G. Kells, D. Meidan, and A. Romito, Topological transitions in weakly monitored free fermions, *SciPost Phys.* **14**, 031 (2023).
- [42] I. Poboiko, P. Pöpperl, I. V. Gornyi, and A. D. Mirlin, Theory of free fermions under random projective measurements (2023), arXiv:2304.03138 [quant-ph].
- [43] M. Fava, L. Piroli, T. Swann, D. Bernard, and A. Nahum, Nonlinear sigma models for monitored dynamics of free fermions (2023), arXiv:2302.12820.
- [44] T. Swann, D. Bernard, and A. Nahum, Spacetime picture for entanglement generation in noisy fermion chains (2023), arXiv:2302.12212.
- [45] J. Merritt and L. Fidkowski, Entanglement transitions with free fermions, *Phys. Rev. B* **107**, 064303 (2023).
- [46] N. Lang and H. P. Büchler, Entanglement transition in the projective transverse field Ising model, *Phys. Rev. B* **102**, 094204 (2020).
- [47] D. Rossini and E. Vicari, Measurement-induced dynamics of many-body systems at quantum criticality, *Phys. Rev. B* **102**, 035119 (2020).
- [48] A. Biella and M. Schirò, Many-body quantum Zeno effect and measurement-induced subradiance transition, *Quantum* **5**, 528 (2021).
- [49] X. Turkeshi, A. Biella, R. Fazio, M. Dalmonte, and M. Schirò, Measurement-induced entanglement transitions in the quantum Ising chain: From infinite to zero clicks, *Phys. Rev. B* **103**, 224210 (2021).
- [50] E. Tirrito, A. Santini, R. Fazio, and M. Collura, Full counting statistics as probe of measurement-induced transitions in the quantum Ising chain (2022), arXiv:2212.09405.
- [51] Z. Yang, D. Mao, and C.-M. Jian, Entanglement in one-dimensional critical state after measurements (2023), arXiv:2301.08255.
- [52] Z. Weinstein, R. Sajith, E. Altman, and S. J. Garratt, Nonlocality and entanglement in measured critical quantum Ising chains (2023), arXiv:2301.08268.
- [53] S. Murciano, P. Sala, Y. Liu, R. S. K. Mong, and J. Alicea, Measurement-altered Ising quantum criticality (2023), arXiv:2302.04325.
- [54] P. Sierant, G. Chiriacò, F. M. Surace, S. Sharma, X. Turkeshi, M. Dalmonte, R. Fazio, and G. Pagano, Dissipative Floquet dynamics: from steady state to measurement induced criticality in trapped-ion chains, *Quantum* **6**, 638 (2022).
- [55] X. Turkeshi, M. Dalmonte, R. Fazio, and M. Schirò, Entanglement transitions from stochastic resetting of non-Hermitian quasiparticles, *Phys. Rev. B* **105**, L241114 (2022).
- [56] Q. Tang and W. Zhu, Measurement-induced phase transition: A case study in the nonintegrable model by density-matrix renormalization group calculations, *Phys. Rev. Research* **2**, 013022 (2020).
- [57] S. Goto and I. Danshita, Measurement-induced transitions of the entanglement scaling law in ultracold gases with controllable dissipation, *Phys. Rev. A* **102**, 033316 (2020).
- [58] Y. Fuji and Y. Ashida, Measurement-induced quantum criticality under continuous monitoring, *Phys. Rev. B*

- 102**, 054302 (2020).
- [59] E. V. H. Doggen, Y. Gefen, I. V. Gornyi, A. D. Mirlin, and D. G. Polyakov, Generalized quantum measurements with matrix product states: Entanglement phase transition and clusterization, *Phys. Rev. Research* **4**, 023146 (2022).
- [60] E. V. H. Doggen, Y. Gefen, I. V. Gornyi, A. D. Mirlin, and D. G. Polyakov, Evolution of many-body systems under ancilla quantum measurements, *Phys. Rev. B* **107**, 214203 (2023).
- [61] O. Lunt and A. Pal, Measurement-induced entanglement transitions in many-body localized systems, *Phys. Rev. Research* **2**, 043072 (2020).
- [62] K. Yamamoto and R. Hamazaki, Localization properties in disordered quantum many-body dynamics under continuous measurement (2023), arXiv:2301.07290.
- [63] S.-K. Jian, C. Liu, X. Chen, B. Swingle, and P. Zhang, Measurement-induced phase transition in the monitored Sachdev-Ye-Kitaev model, *Phys. Rev. Lett.* **127**, 140601 (2021).
- [64] A. Altland, M. Buchhold, S. Diehl, and T. Micklitz, Dynamics of measured many-body quantum chaotic systems, *Phys. Rev. Research* **4**, L022066 (2022).
- [65] C. Noel, P. Niroula, D. Zhu, A. Risinger, L. Egan, D. Biswas, M. Cetina, A. V. Gorshkov, M. J. Gullans, D. A. Huse, and C. Monroe, Measurement-induced quantum phases realized in a trapped-ion quantum computer, *Nat. Phys.* **18**, 760 (2022).
- [66] J. M. Koh, S.-N. Sun, M. Motta, and A. J. Minnich, Measurement-induced entanglement phase transition on a superconducting quantum processor with mid-circuit readout, *Nat. Phys.* 10.1038/s41567-023-02076-6 (2023).
- [67] I. Klich and L. Levitov, Quantum noise as an entanglement meter, *Phys. Rev. Lett.* **102**, 100502 (2009).
- [68] I. Burmistrov, K. Tikhonov, I. Gornyi, and A. Mirlin, Entanglement entropy and particle number cumulants of disordered fermions, *Annals of Physics (NY)* **383**, 140 (2017).
- [69] F. Evers and A. D. Mirlin, Anderson transitions, *Rev. Mod. Phys.* **80**, 1355 (2008).
- [70] See supplemental material at [url] which includes details of the theoretical analysis.
- [71] E. Abrahams, P. W. Anderson, D. C. Licciardello, and T. V. Ramakrishnan, Scaling theory of localization: Absence of quantum diffusion in two dimensions, *Phys. Rev. Lett.* **42**, 673 (1979).
- [72] B. Kramer and A. MacKinnon, Localization: theory and experiment, *Reports on Progress in Physics* **56**, 1469 (1993).
- [73] K. Slevin and T. Ohtsuki, The Anderson transition: Time reversal symmetry and universality, *Phys. Rev. Lett.* **78**, 4083 (1997).
- [74] E. Bettelheim, I. A. Gruzberg, and A. W. W. Ludwig, Quantum Hall transitions: An exact theory based on conformal restriction, *Phys. Rev. B* **86**, 165324 (2012).
- [75] P. Di Francesco, P. Mathieu, and D. Sénéchal, *Conformal Field Theory* (Springer New York, NY, 1997).
- [76] D. J. Gross, Applications of the renormalization group to high-energy physics, in *Methods in Field Theory* (North-Holland Publishing Co., 1976) pp. 141–250.
- [77] X.-G. Wen, Scaling theory of conserved current and universal amplitudes at anisotropic critical points, *Phys. Rev. B* **46**, 2655 (1992).
-

Supplemental Material to “Measurement-induced phase transition for free fermions above one dimension”

In this Supplemental Material, we provide technical details of the analytical calculations used in the main text.

NLSM GENERATING FUNCTIONAL

The generating functional introduced in the main text is given by the path integral over the $SU(R)$ matrix fields \hat{U} as follows [here, $\mathbf{r} = (\mathbf{x}, t)$ and the time integration is constrained to $t < 0$]:

$$\mathcal{Z}[\hat{\Xi}] = \int \mathcal{D}\hat{U} \mathcal{D}\hat{U}^\dagger \exp\left(-\int d^{d+1}\mathbf{r} \mathcal{L}[\hat{U}(\mathbf{r}), \hat{\Xi}(\mathbf{r})]\right) \quad (\text{S1})$$

with the Lagrangian given by Eq. (7) of the main text. To obtain the density-correlation function, one needs to expand it to the second order in $\hat{\Xi}$:

$$C_{ab}(\mathbf{r}_1, \mathbf{r}_2) \equiv -\frac{\delta^2 \ln \mathcal{Z}[\hat{\Xi}]}{\delta \Xi_a(\mathbf{r}_1) \delta \Xi_b(\mathbf{r}_2)} = \frac{g_0}{2v_0} \left(\langle U_{ab}(\mathbf{r}_1) U_{ba}^\dagger(\mathbf{r}_2) \rangle + \delta_{ab} \right) \delta(\mathbf{r}_1 - \mathbf{r}_2) - \frac{g_0^2}{v_0^2} \langle \mathcal{J}_{t,aa}(\mathbf{r}_1) \mathcal{J}_{t,bb}(\mathbf{r}_2) \rangle. \quad (\text{S2})$$

Here, we have introduced the t -component of the Noether current, $\hat{\mathcal{J}}_t(\mathbf{r}) = -\frac{i}{2} \{ \hat{U}^\dagger(\mathbf{r}), \partial_t \hat{U}(\mathbf{r}) \}$, and the average is calculated with respect to the same action without the source term. Further, at the boundary $t \rightarrow 0$, we have $\hat{U}_{ab}(\mathbf{r}) \rightarrow \delta_{ab}$, and thus the boundary correlation function simplifies:

$$C_{ab}(\mathbf{x}_1, \mathbf{x}_2) = \lim_{t_{1,2} \rightarrow 0} \left[\frac{g_0}{v_0} \delta_{ab} \delta(\mathbf{x}_1 - \mathbf{x}_2) \delta(t_1 - t_2) - \frac{g_0^2}{v_0^2} \langle \mathcal{J}_{t,aa}(\mathbf{r}_1) \mathcal{J}_{t,bb}(\mathbf{r}_2) \rangle \right]. \quad (\text{S3})$$

The physical density-correlation function of interest, $C(\mathbf{x}_1, \mathbf{x}_2)$, is defined as [see Eq. (10) of the main text]

$$C(\mathbf{x}) = \overline{\langle \hat{n}(\mathbf{x}), \hat{n}(0) \rangle} / 2 - \overline{\langle \hat{n}(\mathbf{x}) \rangle \langle \hat{n}(0) \rangle}. \quad (\text{S4})$$

It is given by the difference between the diagonal and off-diagonal elements of the matrix $C_{ab}(\mathbf{x}_1, \mathbf{x}_2)$. This was shown for $d = 1$ in Ref. [42], and the derivation is extended straightforwardly to arbitrary d . Utilizing $\text{Tr} \hat{\mathcal{J}}_t = 0$, this yields:

$$C(\mathbf{x}_1, \mathbf{x}_2) = \lim_{t_{1,2} \rightarrow 0} \left[\frac{g_0}{v_0} \delta(\mathbf{x}_1 - \mathbf{x}_2) \delta(t_1 - t_2) - \frac{g_0^2}{v_0^2} \frac{1}{R-1} \sum_a \langle \mathcal{J}_{t,aa}(\mathbf{r}_1) \mathcal{J}_{t,aa}(\mathbf{r}_2) \rangle \right], \quad (\text{S5})$$

which is the last expression in Eq. (10) of the main text.

CORRELATION FUNCTION IN THE GAUSSIAN APPROXIMATION

Employing the exponential parametrization $\hat{U}(\mathbf{r}) = e^{i\hat{\Phi}(\mathbf{r})}$ with a traceless matrix $\hat{\Phi}$, one has $\mathcal{J}_{t,aa}(\mathbf{r}) = \partial_t \Phi_{aa}(\mathbf{r})$ at the boundary. Within the Gaussian approximation, the action for the $\hat{\Phi}$ fields reads:

$$\mathcal{L}_0[\hat{\Phi}] \approx \frac{g}{2} \text{Tr} \left[\frac{1}{v_0} (\partial_t \hat{\Phi})^2 + v_0 (\nabla \hat{\Phi})^2 \right]. \quad (\text{S6})$$

Taking into account the boundary condition $\Phi(x, t = 0) = 0$, the bare correlation function of $\hat{\Phi}$ fields (i.e., that in the Gaussian approximation) is given by:

$$\langle \Phi_{ab}(\mathbf{r}_1) \Phi_{a'b'}(\mathbf{r}_2) \rangle = \left(\delta_{ab'} \delta_{a'b} - \frac{1}{R} \delta_{ab} \delta_{a'b'} \right) \times \int_0^\infty \frac{d\omega}{\pi} \int \frac{d^d \mathbf{q}}{(2\pi)^d} e^{i\mathbf{q}(\mathbf{x}_1 - \mathbf{x}_2)} \sin \omega t_1 \sin \omega t_2 \frac{v_0/g_0}{\omega^2 + v_0^2 q^2}. \quad (\text{S7})$$

Combining this with Eq. (S5), performing the Fourier transformation with respect to the coordinate difference $\mathbf{x}_1 - \mathbf{x}_2$, and making use of the integral representation for the delta-function,

$$\delta(t_1 - t_2) = \int_0^\infty \frac{d\omega}{\pi} \cos \omega(t_1 - t_2), \quad (\text{S8})$$

we obtain:

$$C(\mathbf{q}) = \frac{g_0}{v_0} \int_0^\infty \frac{d\omega}{\pi} \left[1 - \frac{\omega^2}{\omega^2 + v_0^2 q^2} \right] = g_0 |q|. \quad (\text{S9})$$

This is exactly the second part of Eq. (11) of the main text. Finally, performing the inverse Fourier transformation in the spherical coordinates, we obtain:

$$C(\mathbf{x}) = g_0 \int \frac{d^d \mathbf{q}}{(2\pi)^d} |q| e^{i\mathbf{q}\mathbf{x}} = \frac{g_0}{(2\pi)^{d/2}} \frac{1}{x^{d/2-1}} \int_0^\infty q^{d/2+1} J_{d/2-1}(qx) dq = -\frac{\Gamma\left(\frac{d+1}{2}\right)}{\pi^{(d+1)/2}} \frac{g_0}{|\mathbf{x}|^{d+1}}, \quad (\text{S10})$$

where the integral over q was evaluated utilizing the exponential regularization. This is the first part of Eq. (11) of the main text.

The Gaussian-approximation results (S9), (S10) remain valid in the “metallic” phase $\gamma < \gamma_c$, up to a renormalization of the prefactor g_0 due to loop corrections (“weak localization”). The long-range (power-law) behavior (S9), (S10) is a manifestation of the symmetry-broken (Goldstone) character of the $\gamma < \gamma_c$ phase. This behavior leads to a logarithmic $\ln \ell$ enhancement of the entanglement entropy (in comparison to the area-law phase). From this point of view, the scaling in the “metallic” phase may be termed “critical”. We prefer, however, to avoid using the term “critical” with respect to the $\gamma < \gamma_c$ phase, since this might lead to a confusion with the critical point of the transition. Instead, we use in the main text the term “gapless”, which points to the existence of Goldstone modes (“diffusons”) in this symmetry-broken phase.

FLUCTUATIONS OF NUMBER OF PARTICLES

For an arbitrary region A in the d -dimensional space, the second cumulant characterizing fluctuations of the number of particles is given by:

$$\mathcal{C}_A^{(2)} = \int_A d^d \mathbf{x} \int_A d^d \mathbf{y} C(\mathbf{x} - \mathbf{y}) = \int \frac{d^d \mathbf{q}}{(2\pi)^d} |I_A(\mathbf{q})|^2 C(\mathbf{q}), \quad I_A(\mathbf{q}) \equiv \int_A d^d \mathbf{x} e^{i\mathbf{q}\mathbf{x}}. \quad (\text{S11})$$

Consider, for simplicity, the case where A is a ball of radius ℓ . Then the Fourier transform of the indicator function I_A can be calculated explicitly, reading

$$I_A(\mathbf{q}) = \left(\frac{2\pi\ell}{q} \right)^{d/2} J_{d/2}(q\ell). \quad (\text{S12})$$

It is a rapidly oscillating function for momenta $q \sim 1/\ell$; as we are interested in the asymptotic behavior at $\ell \rightarrow \infty$, we can average over these oscillations, yielding:

$$|I_A(\mathbf{q})|^2 \approx (2\pi)^d \frac{\ell^{d-1}}{\pi q^{d+1}} \quad (\text{S13})$$

and thus

$$\mathcal{C}_\ell^{(2)} \approx \frac{\sigma_{d-1} \ell^{d-1}}{\pi} \int_{\sim 1/\ell}^{\sim 1/\ell_0} dq \frac{C(\mathbf{q})}{q^2}, \quad (\text{S14})$$

with $\sigma_{d-1} = 2\pi^{d/2}/\Gamma(d/2)$ a surface of $d-1$ -dimensional unit sphere. Here, we have also introduced an IR cutoff at the scale $\sim 1/\ell$, where oscillations are not developed, and the UV cutoff at the scale $\sim 1/\ell_0$, where the NLSM starts to be applicable. This equation can also be rewritten in a RG-like form as follows:

$$\frac{d\mathcal{C}_\ell^{(2)}}{d \ln \ell} = (d-1)\mathcal{C}_\ell^{(2)} + \alpha Z^2(\ell)G(\ell) \quad (\text{S15})$$

with $\alpha = O(1)$ being geometry-dependent constant and $G(\ell)$ and $Z(\ell)$ being dimensionless coupling constants governed by RG equations (13), (14) from the main text. For the Gaussian approximation (S9), we obtain

$$\mathcal{C}_\ell^{(2)} \approx \frac{g_0}{\pi} \sigma_{d-1} \ell^{d-1} \ln \frac{\ell}{\ell_0}, \quad (\text{S16})$$

which is Eq. (12) of the main text. This result can be generalized to a region A of an arbitrary shape with characteristic size ℓ ; the result is given by Eq. (S16) with $\sigma_{d-1} \ell^{d-1}$ replaced by the area S_A of the region A .

COVARIANCE OF PARTICLE NUMBER AND MUTUAL INFORMATION.

Equation (S5) shows us that the density correlation function is in fact given (up to a “contact” term) by a correlation function of Noether currents \mathcal{J}_t associated with the $SU(R)$ symmetry of the corresponding NLSM. Within the context of NLSM for disordered systems and Anderson localization, such correlation function is formally equivalent to the local conductivity calculated between two points \mathbf{x} and \mathbf{x}' on the boundary of the $(d+1)$ -dimensional sample, where we have simply identified time with another spatial dimension. Moreover, the “absorbing boundary condition” $\hat{U}(\mathbf{x}, t=0) = \hat{\mathbb{I}}$ can also be translated to the ideal conducting leads attached to the sample in the Anderson localization setup.

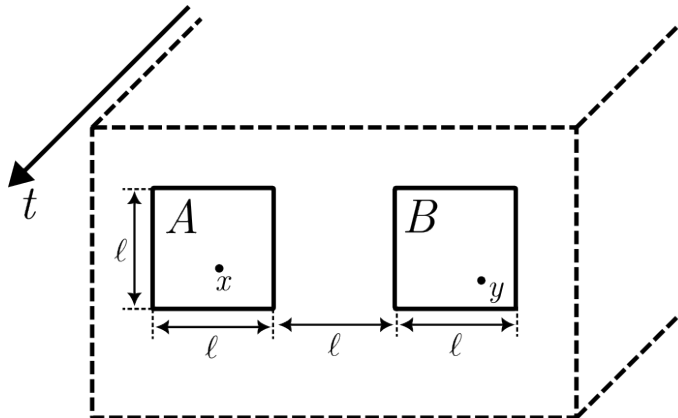


FIG. S4. Geometry for calculation of covariance G_{AB} of number of particles in regions A and B of size $\ell \times \ell$ each, separated by a distance $\sim \ell$. At the critical point, G_{AB} should be scale-invariant, i.e. independent of ℓ , for $1 \ll \ell \ll L$. Moreover, for a given geometry (e.g., square regions A and B of size $\ell \times \ell$ separated by a distance ℓ , as in the figure), the value of G_{AB} at criticality is a *universal* constant (i.e., it does not depend on microscopic details of the model but only on its spatial dimensionality and symmetries).

Pushing forward this formal analogy, it then becomes natural to consider a “two-terminal conductance”:

$$G_{AB}(\ell) = - \int_A d^d \mathbf{x} \int_B d^d \mathbf{y} C(\mathbf{x} - \mathbf{y}) \quad (\text{S17})$$

for the geometrical setup sketched on Fig. S4. At the critical point, $\gamma = \gamma_c$, the conductance G_{AB} is expected to be scale invariant, i.e., independent of the subsystem size ℓ , which is only possible provided the following scaling for the density correlation function at the critical point:

$$C(\mathbf{x} - \mathbf{y}) \sim - \frac{G_c}{|\mathbf{x} - \mathbf{y}|^{2d}} \quad (\text{critical point}). \quad (\text{S18})$$

As discussed in the main text, the scaling (S18) also follows from the fact that $C(\mathbf{x} - \mathbf{y})$ is a correlation function of conserved (Noether) currents. In the Fourier domain, Eq. (S18) corresponds to $C(\mathbf{q}) \sim G_c q^d$ for $d < 2$, thus implying the critical index $\zeta = 0$. Note that for $d = 2$ a logarithmic correction to momentum-space scaling is expected: $C(\mathbf{q}) \sim G_c q^2 \ln(1/ql_0)$. We do not see evidences of such a logarithmic factor in our numerical analysis of $C(\mathbf{q})$. Presumably, a clear numerical observation of this logarithmic correction requires considerably larger system sizes.

Using the behavior of the correlation function $C(\mathbf{x})$ in the “metallic” phase, $C(\mathbf{x}) \propto 1/|\mathbf{x}|^{d+1}$ and in the “localized” phase, $C(\mathbf{x}) \propto e^{-|\mathbf{x}|/\ell_{\text{corr}}}$ (see main text), we obtain

$$G_{AB}(\ell) \sim \begin{cases} \ell^{d-1}, & \text{“metal”} \\ G_c, & \text{critical point} \\ e^{-\ell/\ell_{\text{corr}}}, & \text{“insulator”}, \end{cases} \quad (\text{S19})$$

as stated in the main text at the end of the section “Exactness of $\zeta = 0$. Mutual information”. This scaling behavior of G_{AB} in the problem of monitored free fermions is fully analogous to the behavior of the two-terminal conductance of a disordered system around the Anderson transition.

According to Eq. (S4), the quantity G_{AB} in the present context is equal (up to a minus sign) to the covariance of the particle numbers in two regions A and B,

$$G_{AB} = - \overline{\langle \hat{N}_A \hat{N}_B \rangle}. \quad (\text{S20})$$

Moreover, one can show that it is related to the mutual information between these two regions, which is formally defined as:

$$I(A : B) = \mathcal{S}_E(A) + \mathcal{S}_E(B) - \mathcal{S}_E(A \cup B), \quad (\text{S21})$$

with $\mathcal{S}_E(C)$ being the standard entropy of entanglement between the region C and the rest of the system. Using the Klich-Levitov relation for the entanglement entropy [Eq. (6) of the main text] and truncating the series with the first term [see the justification of this approximation below Eq. (6) of the main text], we obtain:

$$I(A : B) \approx \frac{2\pi^2}{3} G_{AB}. \quad (\text{S22})$$

Thus, the scaling (S19) is expected to be applicable to the mutual information $I(A : B)$ as well, as pointed out in the main text.

Finally, it is worth emphasizing universality of G_{AB} and $I(A : B)$ at criticality in the considered problem. Specifically, let us fix the dimensionality d and geometry of A and B (e.g., $d = 2$ with square regions A and B of size $\ell \times \ell$ separated by a distance ℓ , as in Fig. S4). Then, using conventional argumentation in theory of critical phenomena, one concludes that G_{AB} and $I(A : B)$ are universal constants independent of microscopic details of the model.